13th World Conference on Earthquake Engineering
Vancouver, B.C., Canada
August 1-6, 2004
Paper No. 96

A DIRECT DISPLACEMENT BASED DESIGN APPROACH FOR UNBONDED POST-TENSIONED MASONRY WALLS

G.D. WIGHT[1] and M.J. KOWALSKY[2]

SUMMARY

Post-tensioned masonry walls exhibit superior earthquake performance due to increased in-plane strength and the absence of residual lateral displacement at conclusion of the seismic loading. The Direct Displacement-Based Design (DDBD) approach aims to provide the engineer with the tools needed to design a structure to achieve a pre-defined level of lateral deformation under a pre-defined level of earthquake intensity. This paper details the development of a DDBD procedure to assist in the design of unbonded post-tensioned masonry shear walls. Results from the method are compared with actual data obtained by subjecting two full-scale concrete masonry walls, of differing aspect ratio, to a variety of ground accelerations on a shake table at North Carolina State University. A design example that highlights the steps involved in applying this design approach to an actual structure is included to demonstrate the simplicity of the method.

INTRODUCTION

The use of unbonded post-tensioning in structural systems to resist lateral forces due to earthquakes was first proposed by Priestley [1]. Since then the approach has been used for the design of concrete buildings [2], concrete masonry walls [3], steel moment frames [4, 5], and clay brick masonry walls [6].

The primary advantage that unbonded post-tensioning provides involves a 'self-correcting' characteristic where structural members will return to the undeformed configuration after seismic attack while sustaining little damage. The self-corrective nature is a direct result of the unbonded post-tensioning. As long as the reinforcing retains some level of residual pre-stress force, the force in the bars will cause the structural members to return to the plumb position. In addition to the self-corrective nature, structures with unbonded post-tensioning tend to sustain very little damage due to lateral forces, and damage is typically confined to the wall lower corners, as no flexural tension stresses are induced in the structural member.

[1] PhD Student, University of Auckland, New Zealand, Email: gwight@xtra.co.nz
[2] Assistant Professor, North Carolina State University, Email: kowalsky@eos.ncsu.edu

OVERVIEW OF DIRECT DISPLACMENT-BASED DESIGN APPROACH

The Direct Displacement-Based Design (DDBD) [7, 8] approach aims to provide the engineer with the tools needed to design a structure to achieve a pre-defined level of lateral deformation under a pre-defined level of earthquake intensity. Since damage correlates well with lateral deformation, the DDBD approach allows the engineer to control structural performance for a variety of earthquake intensity levels, thus making the DDBD approach a viable performance-based design approach. DDBD utilizes the concept of equivalent viscous damping as defined by Jacobsen [9, 10], and the substitute structure approach advanced by Gulkan and Sozen [11] and Shibata and Sozen [12]. The DDBD procedure was initially developed for single degree of freedom reinforced concrete columns [7], and was subsequently developed for multi-span bridge structures [13] and multi-story building frames [8]. In all cases, dynamic inelastic time history analysis has shown that analysis displacements generally agree with those assumed in the design. The basic steps of the DDBD approach are shown below.

DDBD STEPS

Step 1: Selection of Target Displacement

The target displacement for the design of a structural system can be defined by strain-based damage criteria, or directly by drift limits. In the case of masonry walls with unbonded post-tensioning, target displacements may be established by three criteria: (1) Masonry compression strain, (2) Lateral drift ratio, and (3) Post-tensioning steel tension strain.

Step 2: Selection of Seismic Demand

The seismic demand for DDBD is a displacement response spectra generated for several levels of viscous damping. Although displacement response spectra from real earthquake records have been used for validation studies of DDBD, design is likely to proceed through the use of simplified and smoothed code-based design spectra. Utilizing the IBC code, the 5% damped displacement response spectra can be directly obtained from the 5% damped acceleration spectra by multiplying the spectral ordinates by Eq. 1. Displacement response spectra for damping levels other than 5% can then be obtained by multiplying the 5% damped curve by Eq. 2 [14].

$$Sd_{5\%} = \frac{Sa_{5\%} T^2}{4\pi^2} \qquad \text{(Eq. 1)}$$

$$Sd_{X\%} = Sd_{5\%} \sqrt{\left(\frac{7}{2+\zeta_{eff}}\right)} \qquad \text{(Eq. 2)}$$

Step 3: Calculation of Structure Effective Period

Once the target displacement is selected in Step 1, and the demand established in Step 2, the effective period at maximum response is obtained as shown in Fig. 1a. Note that in Fig. 1a, the engineer enters with the value for the target displacement, Δ_{target}, and reads across to the appropriate response curve and down to determine the effective period, T_{eff}. The response curve that is selected is a function of the level of equivalent viscous damping for the system under consideration. Relations for equivalent viscous damping can be defined as a function of lateral drift or ductility for different material and systems, and is assumed to be a function only of the hysteretic loop shape. Fig. 1b illustrates some typical relationships between damping and drift ratio for reinforced masonry walls and masonry walls with unbonded post-tensioning.

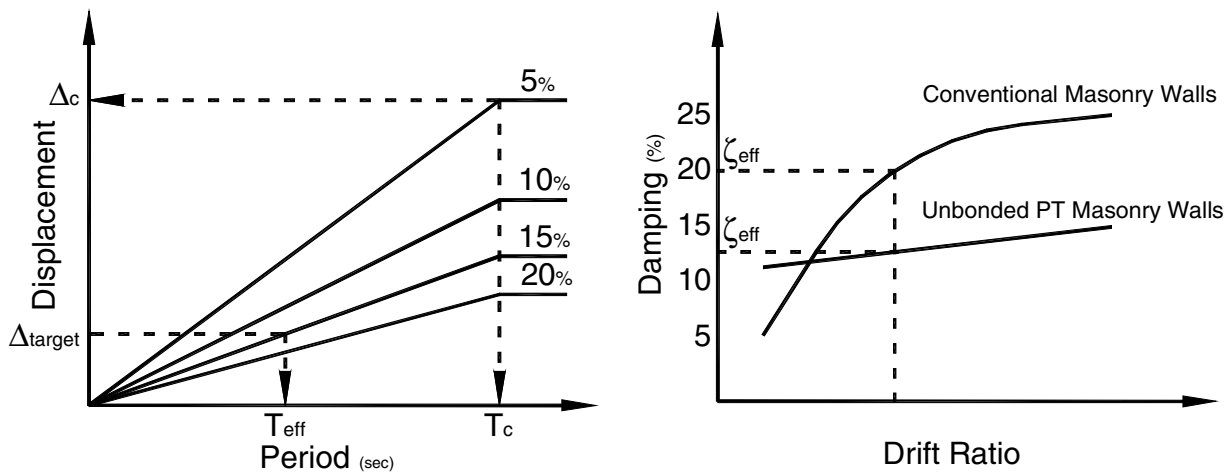

(a) Obtaining T_{eff} from displacement response spectra **(b) Equivalent viscous damping**

Figure 1: Calculating effective period

Step 4: Calculation of Design Base Shear

Once the effective period of the substitute structure is obtained in Step 3, the effective stiffness is readily obtained with Eq. 3. It is important to note that the effective stiffness of the substitute structure is defined as the secant stiffness to maximum response, as shown in Fig. 2. The design base shear force at the design limit state is then obtained by multiplying the effective stiffness by the target displacement (Eq. 4) as shown in Fig. 2.

$$K_{eff} = \frac{4\pi^2 m_{eff}}{T_{eff}^{\ 2}} \qquad \text{(Eq. 3)}$$

$$V_b = K_{eff}\Delta_{target} \qquad \text{(Eq. 4)}$$

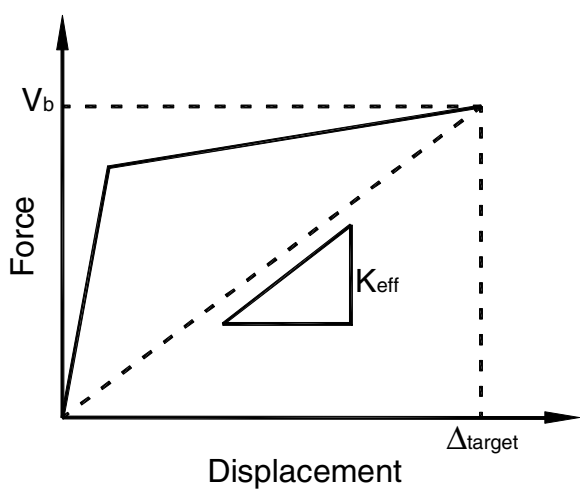

Figure 2: Obtaining the design base shear force

Step 5: Structural Analysis and Design
With the design base shear force known, structural analysis is conducted to determine the required strength of members in the structure. Members are then proportioned accordingly to resist the seismic demands in terms of strength and deformation.

SIMPLIFIED DESIGN EXPRESSION FOR DDBD

The steps previously described can be combined into one expression for the design base shear force which is shown below as Eq. 5.

$$V_b = \frac{4\pi^2 M_{sys}}{\Delta_{sys}} \frac{\Delta_c^2}{T_c^2} \frac{7}{2+\zeta_{eff}} \qquad \text{(Eq. 5)}$$

In Eq. 5, the variables Δ_c and T_c represent the corner point spectral displacement and period as shown in Fig. 1a. The corner point period has been shown to be a function of moment intensity and epicentral distance [15]. Typical values of the corner point period range from 2-6 seconds, with a value of 4 seconds often utilized. The corner point displacement is obtained directly from the spectral acceleration. In the case of the IBC code, the corner point displacement is obtained from Eq. 6.

$$\Delta_c = \frac{Sd_1 T_c g}{2\pi^2} \qquad \text{(Eq. 6)}$$

TARGET DISPLACEMENTS FOR POST-TENSIONED MASONRY WALLS

Criteria
Target displacements for post-tensioned masonry walls can be established based on material strains or as absolute drift limits that define key points along the force-deformation response of the structure. Application of the DDBD procedure previously discussed applies equally well, regardless of how the target displacements are selected. However, it is most likely that target displacements defined by tension strains in the post-tensioning tendons will be most critical, therefore this criteria is further investigated in this paper.

Drift Limits based on Steel Strain
Consider Fig. 3 which represents a masonry wall with unbonded post-tensioning tendons subjected to a lateral force. The elongation of a wall tendon, Δ_i, due to rocking deformation, can be related to the wall top displacement by Eq. 7 where 'c' represents the neutral axis depth and 'x_i' the distance between the wall edge and tendon. The elongation of the tendon can also be defined by Eq. 8 where L_{un} represents the unbonded length of tendon and ε_{rock} represents the strain induced in the tendon due to rocking deformation.

$$\frac{\Delta_T}{H_w} = \frac{\Delta_i}{x_i - c} \qquad \text{(Eq. 7)}$$

$$\Delta_i = \varepsilon_{rock} L_{un} \qquad \text{(Eq. 8)}$$

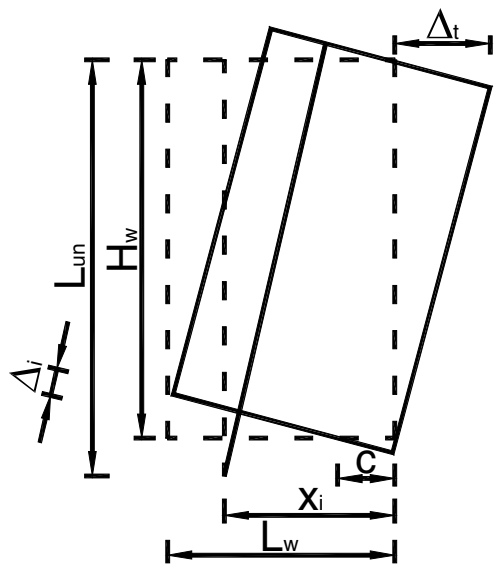

Figure 3: Tendon strain increase due to rocking

The unbonded length, L_{un}, can be expressed by Eq. 9, and the values for c and x_i can be related to the wall length by Eqs. 10 and 11. Introducing those constants allows Eq. 7 to be rewritten as Eq. 12. Defining A_r as the wall aspect ratio (H_w/L_w) allows Eq. 12 to be expressed as Eq. 13.

$$L_{un} = \gamma H_w \qquad \text{(Eq. 9)}$$

$$x_i = \alpha L_w \qquad \text{(Eq. 10)}$$

$$c = \beta L_w \qquad \text{(Eq. 11)}$$

$$\frac{\Delta_T}{H_w} = \frac{\varepsilon_{rock}\gamma H_w}{(\alpha - \beta)L_w} \qquad \text{(Eq. 12)}$$

$$\frac{\Delta_T}{H_w} = \frac{\varepsilon_{rock}\gamma}{(\alpha - \beta)} A_r \qquad \text{(Eq. 13)}$$

Eq. 13 represents the wall drift ratio (top displacement divided by wall height) as a function of rocking strain in a tendon, ε_{rock}, and aspect ratio, A_r. Eq. 13 also shows that the critical tendon, in a wall with multiple tendons, will be that positioned the furthest from the compression zone, giving the largest value of α and hence the smallest value of Δ_T for a given tendon strain. The total strain in any tendon at any point in time is comprised of two components: (1) Initial strain due to the applied post-tensioning force, ε_{pt}, and (2) Strain induced due to rocking deformation, ε_{rock}.

In order to determine the target displacement consistent with a prescribed level of total tension strain, ε_t, in the tendons, it is first necessary to select the initial pre-strain, ε_{pt}. The rocking strain, ε_{rock}, to achieve the prescribed total tension strain, ε_t, is then obtained by subtracting the strain due to the initial pre-stress from the target total strain as shown in Eq. 14.

$$\varepsilon_{rock} = \varepsilon_t - \varepsilon_{pt} \qquad \text{(Eq. 14)}$$

If it is assumed that γ=1.25, and that the rocking strain for the yield limit state is $0.8\varepsilon_y$, then Eq. 13 reduces to Eq. 15. Assuming a yield strain in the post-tensioning steel of 0.004, the drift ratio can be plotted as a function of aspect ratio for various values of (α-β), with the results shown in Fig. 4.

$$\frac{\Delta_T}{H_w} = \frac{\varepsilon_y}{(\alpha - \beta)} A_r \qquad \text{(Eq. 15)}$$

From Fig. 4, as the distance between the extreme tendon and neutral axis depth increases, the allowable drift ratio decreases. Therefore, placing the tendons closer to the center of the walls will allow the walls to accommodate a larger lateral drift ratio prior to reaching the prescribed tendon strain limit state.

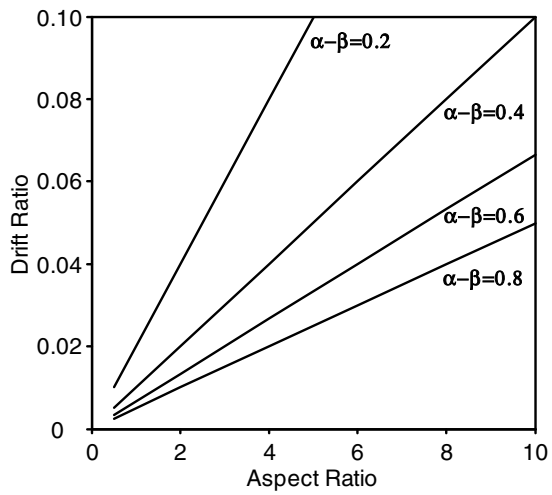

Figure 4: Drift ratio verses aspect ratio for ε_s=0.8ε_y and ε_y=0.004

EQUIVALENT VISCOUS DAMPING

The equivalent viscous damping is a 'measure' of the energy dissipated during a seismic attack and consists of two parts: (1) viscous damping and (2) hysteretic damping. Fig. 1(b) compares the equivalent viscous damping versus drift ratio of a typical conventionally reinforced masonry wall with one that has unbonded post-tensioning reinforcement. One thing that is evident upon inspection of the figure is that the equivalent viscous damping of the unbonded post-tensioned wall is lower than that of the conventionally reinforced wall at higher drift ratios and the opposite is true at lower drifts. While having a damping effect at lower drift ratios is an advantage to unbonded post-tensioned masonry walls, there will be increased lateral deformations and therefore greater tensile strains in the post-tensioning tendons and compressive strains in the masonry at higher drift ratios. With proper design the latter can be avoided.

SAMPLE TEST RESULTS

Two post-tensioned concrete masonry walls were subjected to a variety of ground excitations on a shake table at North Carolina State University. The walls, referred to as wall 1 and wall 2, had lengths of 1016 mm (40 in.) and 813 mm (32 in.) respectively. Both walls were 2438 mm (96 in.) high and 143 mm (5 5/8 in.) wide, and were prestressed with a single Dywidag threadbar, located at the wall center, having a diameter of 16 mm and a specified yield strength of 163 kN. The variety of acceleration records used included both pulse and reversal type records with long and short durations. Some records required scaling of time to ensure the maximum ground displacement did not exceed the table maximum of 127 mm. For additional results from the shake table testing of post-tensioned concrete masonry walls, refer to Wight et. al [16].

Fig. 5 shows a single force-displacement loop (FD) for wall 1. This was derived using the equation of motion for a SDF system subjected to an external force, which is shown in Eq. 16, where m, c and k are the seismic mass, damping coefficient and stiffness respectively and $\ddot{u}$, $\dot{u}$, u and $\ddot{u}_g$ are the relative wall acceleration, relative wall velocity, relative wall displacement and ground acceleration respectively.

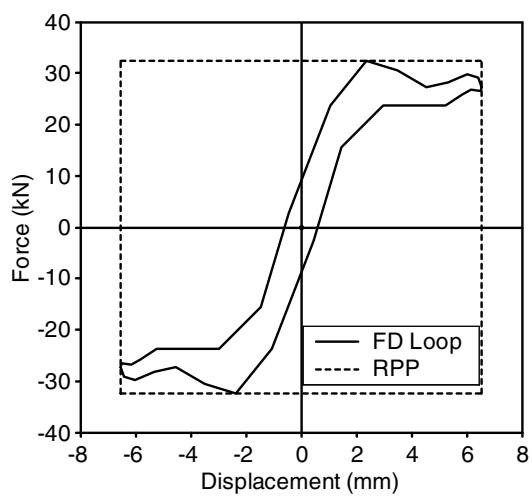

Figure 5: A single force-displacement loop for wall 1

$$m\ddot{u} + c\dot{u} + ku = -m\ddot{u}_g \qquad \text{(Eq. 16)}$$

It can be shown that the lateral force exerted on the wall is equal to the seismic mass multiplied by the absolute acceleration, measured at the wall top, plus the damping term, as shown in Eq. 17.

$$ku = -(m(\ddot{u} + \ddot{u}_g) + c\dot{u}) \qquad \text{(Eq. 17)}$$

Single loops were then extracted from the FD plot for the cycles in which the wall reached its maximum and minimum top of wall displacements during the run. Typically these loops were not symmetric about the origin, therefore the larger half loop was taken and reflected about the origin, creating a symmetric loop and allowing easier calculation of damping. Equivalent viscous damping was calculated using

Eq. 18, where A_{loop} is the area enclosed by the FD loop and A_{RPP} is the area of a rectangular perfectly plastic (RPP) loop that goes through the maximum and minimum FD points, as shown in Fig. 5.

$$\zeta = \frac{2}{\pi}\frac{A_{loop}}{A_{RPP}} \qquad \text{(Eq. 18)}$$

The yield point or the displacement that corresponds to a ductility of 1, was defined as the point at which the wall rocked, resulting in an increase in prestress force and shown in Fig. 5 as the point at which the bilinear curve changed stiffness. Yield displacements of 2.2 mm and 2.8 mm were found for walls 1 and 2 respectively. Dividing the maximum FD loop displacement by the yield displacement gives the level of ductility and when plotted against equivalent viscous damping, results in Fig. 6. Since Eq. 17 includes the viscous damping term, the value of equivalent viscous damping found using Eq. 18, and plotted in Fig. 6, includes both viscous and hysteretic damping. Calculation of viscous damping from the last few cycles of the decay curves for each wall, found a value of 5% for both walls

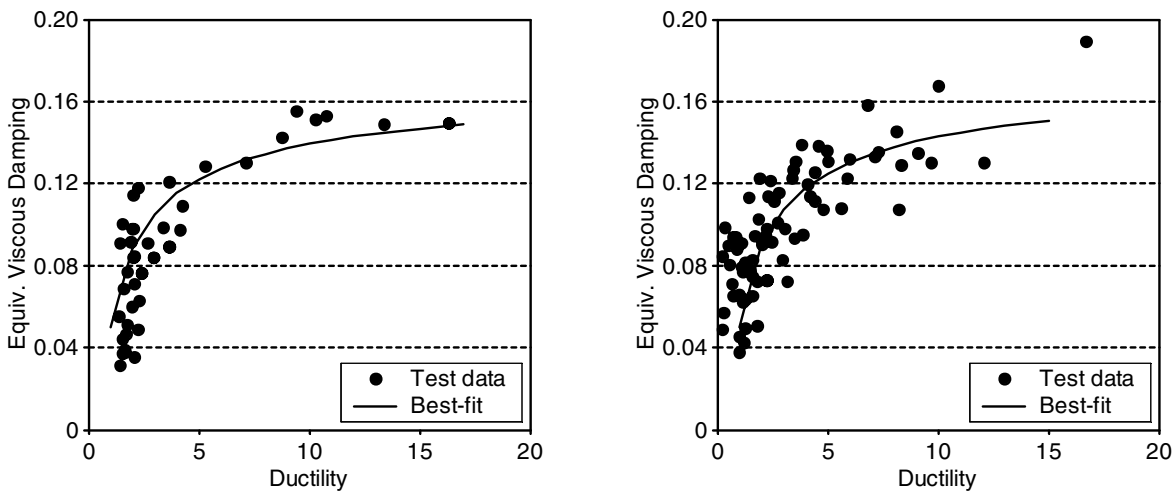

(a) Wall 1 **(b) Wall 2**

Figure 6: Damping – ductility relationship

The best-fit line, shown in Fig. 6, was optimized using the least squares method and has the form shown in Eq. 19 where the constant, a, has values of 0.1305 and 0.1356 for walls 1 and 2 respectively and $\zeta_{vis.}$ is equal to 0.05.

$$\zeta_{evd} = \zeta_{vis.} + a\left(1 - \frac{1}{\sqrt{\mu}}\right) \qquad \text{(Eq. 19)}$$

The previously outlined DDBD approach can be applied to the shake table test results to determine the accuracy of the method. By taking the absolute peak displacement, from each run, and the corresponding lateral force, the effective stiffness and effective period can be calculated. Generating the displacement spectra from the ground acceleration trace recorded on the table surface during each run, and entering the spectra with the calculated effective period, gives a spectral displacement. Fig. 7 shows the ratio of predicted wall displacement using the DDBD approach to measured wall displacement from test data,

plotted against effective period, for both walls tested. The method predicted the displacement for wall 2 with sufficient accuracy, but resulted in greater scattered for wall 1. Combining all the data points gives an average ratio of 1.016 with a standard deviation of 0.326. Though the average is excellent the large scatter requires further investigation by including additional test results and running time history analyses using the Ruaumoko Ring-Spring model [17]. A parallel study is currently underway at North Carolina State University [18], investigating damping using the Ring-Spring model. A variety of earthquake records were used showing a good match between computer model and DDBD prediction, so ultimately this study could be included with the shake table test data to reduce the scatter in results.

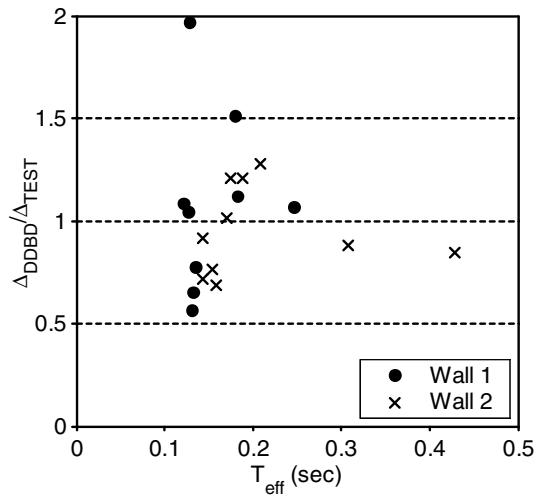

Figure 7: Comparison between DDBD wall displacements and test data

EXAMPLE

To demonstrate the application of the DDBD approach for masonry walls with unbonded tendons, the following design example is discussed.

Step 1: Initial Input Parameters

The example wall is shown in Fig. 8 and is 8 m tall by 4 m long. The yield stress of the post-tensioning reinforcement is 800MPa, while the compression strength of the masonry is 20 MPa. The wall thickness is 190 mm. The wall carries an axial load of 200 kN, and the inertia mass is 50000 kg. The 5% damped displacement response spectra is defined by a corner point period of T_c = 4 sec, and the corner point displacement is Δ_c = 600 mm. The unbonded length of tendon is $1.1l_w$, and the tendon is to achieve a strain of ε_y (0.004) under the design level event, which in this case is defined as a drift of 1.5%. An equivalent viscous damping of 12% is assumed for design, and the post-tensioning tendons are to be grouped at the two locations shown in Fig. 8, being 2.2 m and 1.8 m from the wall end.

Step 2: Select Target Displacement

The target displacement at the center of seismic force is found by multiplying the specified drift ratio by the seismic height giving a value of 0.080 m. Note that the total wall height is multiplied by 2/3 to determine the center of seismic force based on a triangular distribution of forces. While this is an approximation, it has been shown to be reasonably accurate [19], particularly for buildings greater than 2 storeys in height.

Step 3: Calculate Design Base Shear
A design base shear, of 229 kN, was calculated using Eq. 5. Therefore the required moment strength is equal to 1219 kN.m.

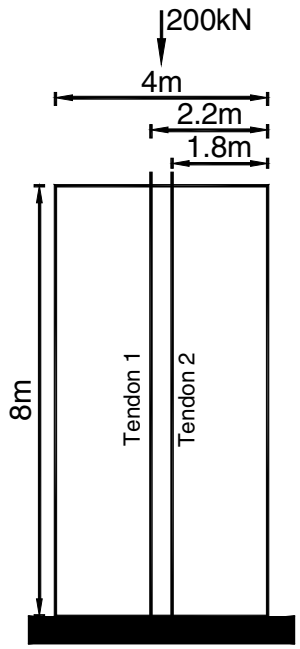

Figure 8: Example wall dimensions

Step 4: Calculate Required Area of Post-tensioning Steel
Given the wall displacement profile, the increase in tendon strain can be derived, and knowing the required wall moment strength, the area of post-tensioning steel calculated. The neutral axis depth is a function of the forces acting on the wall, which is unknown at this stage, but from past experimental results, a good starting point is to use 10% of the wall length, in this case 0.4 m. Using Eq. 13, the increase in strain due to rocking for the tendons in the two locations, is found to be ε_{1rock}=0.00307 and ε_{2rock}=0.00239, where tendon 1 is the critical tendon furthest from the compression zone. Substituting the value for ε_{1rock} into Eq. 14, gives a value of initial prestrain, ε_{pt}, of 0.00093 (0.23ε_y). Therefore the tendon strains at the design drift level are 0.004 and 0.00332 for tendons 1 and 2 respectively. Moment equilibrium can now be performed, with the only unknown being the area of post-tensioning steel required, which is found to be 306 mm^2 at each location.

Step 5: Check Assumed Neutral Axis and Iterate
Assuming a triangular stress block and a wall compressive strength of 20 MPa, the neutral axis is found to be 0.341 m. A series of iterations are now performed before arriving at the final values of 306 mm^2 for the area of post-tensioning steel required at each location, and an initial prestressing tendon strain of 0.00083 or 0.21ε_y. Though this solution satisfies the design requirements for this limit state, the solution needs to be checked at other limit states which may govern, such as serviceability.

DISCUSSION AND FUTURE WORK

This paper has outlined the steps of DDBD and developed a method for designing post-tensioned masonry walls using the DDBD procedure. The design method was compared with shake table test data showing a satisfactory match, but it is recognized that the data set size was small and further verification of the method and damping model used is required. This will be carried out using addition shake table test data and time-history analysis results from Ruaumoko. The test data set will not only be expanded to include other wall aspect ratios, but also different levels of initial prestress.

CONCLUSIONS

A DDBD approach for post-tensioned masonry walls is developed and shown in an example to be simple to apply.

Damping-ductility curves were derived from shake table test data and indicate the relatively low levels of equivalent viscous damping inherent in a post-tensioned wall system.

The test data was compared against predicted wall displacements from the DDBD approach, showing a good match. Though these results are encouraging, further work is planned to expand the data set for design approach verification.

ACKNOWLEDGEMENTS

The authors would like to acknowledge the support of the National Science Foundation (NSF) through grant #0080210. In addition, the support of North Carolina State University, Department of Civil Engineering is appreciated. Several local industry members are also thanked: Eric Johnson of the Carolinas Brick Association, Cody Cress of General Shale, Frank Werner of Adams Products Company and Sika for material donations, Danks Burton of Pinnacle Masonry, Doug Burton of Whitman Masonry, and Calvin Brodie of Brodie Contractors for mason's labor support, and John Little and Gary Rhodes of AmeriSteel. The support of the National Concrete Masonry Association for the research on concrete masonry is greatly appreciated. Fulbright New Zealand, the Todd Foundation and the University of Auckland are thanked for their financial assistance. We would also like to thank Jerry Atkinson, the technician at the Constructed Facilities Laboratory at NC State without whom this work would not have been possible.

REFERENCES

1. Priestley M.J.N. “Seismic design philosophy for precast concrete frames.” Struct. Eng. Int., IABSE, Zurich, Switzerland, 1996; 6(1): 25-31.
2. Priestley M.J.N., Sritharan S., Conley J.R., Pampanin S. “Preliminary results and conclusions from the PRESSS five-storey precast concrete test building.” PCI Journal 1999; 44(6): 42-67.
3. Laursen P.T., Ingham J.M. “Structural testing of single-storey post-tensioned concrete masonry walls.” J. of the Masonry Society 2001; 19(1): 69-82.
4. Ricles J.M., Sause R., Garlock M.M., Zhao C. “Posttensioned seismic-resistant connections for steel frames.” J. Struct. Eng. 2001; 127(2): 113-121.
5. Christopoulos C., Filiatrault A., Uang C-M., Folz B. “Posttensioned energy dissipating connections for moment-resisting steel frames.” J. Struct. Eng. ASCE 2002; 128: 1111-1120.
6. Rosenboom O.A., Kowalsky M.J. “Reversed in-plane cyclic behaviour of post-tensioned clay brick masonry walls.” ASCE J. Struct. Eng. 2004; 130(5).

7. Kowalsky M.J., Priestley M.J.N., MacRae G.A. "Displacement based design of RC bridge columns in seismic regions." J. Earthquake Eng. and Struct. Dynamics 1995; 24: 1623-1643.
8. Priestley M.J.N., Kowalsky M.J. "Direct displacement based design of concrete buildings." Bull. New Zealand Society for Earthquake Eng. 2000; 33(4): 421-444.
9. Jacobson L.S. "Steady forced vibrations as influenced by damping." ASME Transactione 1930; 52(1): 169-181.
10. Jacobsen L.S. "Damping in composite structures." 2nd World Conference on Earthquake Engineering, Japan, 1960: 1029-1044.
11. Gulkan P., Sozen M.A. "Inelastic responses of reinforced concrete structures to earthquake motions." Proc. of the ACI 1974; 71(12): 605-610.
12. Shibata A., Sozen M. "Substitute structure method for seismic design in R/C." J. Struct. Division ASCE 1976; 102(ST1): 1-18.
13. Kowalsky M.J. "A displacement-based approach for the seismic design of continuous concrete bridges." Earthquake Eng. and Struct. Dynamics 2002; 31: 719-747.
14. CEN "European Prestandard ENV1998:Eurocode 8 – Design provision for earthquake resistance of structures." Comite Europeen de Normalisation, Brussels, 1996.
15. Faccioloi E., Paolucci R., Rey J. "Displacement spectra for long periods" Earthquake Spectra 2004; in press.
16. Wight G.D., Ingham J.M., Kowalsky M.J. "Shake table testing of post-tensioned concrete masonry walls." Proc. of 13th International Brick and Block Masonry Conference, Amsterdam, 2004; in press.
17. Carr A.J. "RUAUMOKO – Inelastic dynamic analysis program." Christchurch, New Zealand: Dept. of Civil Engineering, Univ. of Canterbury. 2000.
18. Dwairi H.M., Kowalsky M.J. "Investigation of Jacobson's equivalent viscous damping approach as applied to displacement based seismic design". Proc. of the 13th World Conference on Earthquake Engineering, Vancouver, Canada, 2004: Paper no. 228.
19. Paulay T., Priestley M.J.N. "Seismic design of reinforced concrete and masonry buildings." New York: John Wiley, 1992.